SAR Image Segmentation Using the Roughness Information

F. A. Ávila Rodrigues, J. F. S. Rocha Neto, R. C. Pinheiro Marques, F. N. Sombra de Medeiros, and J. Santos Nobre

***Abstract*—Image segmentation can be applied to a broad class of different problems. However, it is not usually a simple task for synthetic aperture radar (SAR) images due to the presence of speckle. Given the importance of SAR images in remote sensing problems, this letter introduces a simplified and general methodology to achieve SAR image segmentation by using the estimated roughness parameters of SAR data modeled by G_I^0 and G_A^0 distributions, instead of directly processing the speckled images. In this letter, we adopted the log-cumulants method for the roughness parameter estimation. The performance evaluation of the results was attained in terms of the error of segmentation and cross-region fitting measures for synthetic and real SAR images, respectively. With regard to synthetic images, we performed Monte Carlo experiments which confirmed the suitability of SAR image segmentation by means of roughness parameters. The results showed that the methodology provides a feasible input to SAR image segmentation algorithms which also include thresholding-based methods. The proposed approach accomplished satisfactory results for the most interesting and critical study case, i.e., the single-look images, which are markedly affected by speckle.**

***Index Terms*—Log cumulants, roughness parameter, segmentation, synthetic aperture radar (SAR) image, thresholding, G_A^0 distribution, G_I^0 distribution.**

I. Introduction

IMAGE segmentation is one of the most important tasks in digital image processing. Moreover, it is widely used in different research fields such as synthetic aperture radar (SAR) image applications, machine vision, medical imaging, and industrial applications, to name but a few. Segmentation methods based on thresholding generally use the most evident image information, i.e., intensity of pixels. Thresholding is a quite simple and useful segmentation approach because it is a data-reduction step, and therefore, it produces a binary image representation. Binary images are readily manipulated to produce higher level descriptions of the scenes and objects, such as borders and relational graphs [1].

However, in the presence of noise, the intensity distribution of pixels is not bimodal or multimodal, and thus, thresholding-based techniques cannot be directly applied to gray-level images. In fact, these techniques are suitable when the gray level of pixels which belong to an object (foreground) is substantially different from background pixels [2]. This may occur, for example, in high-contrast images. Therefore, these are some of the challenges in applying thresholding-based techniques to noisy images. To tackle some of these issues, we propose a methodology for automatic segmentation of SAR images which encompasses data model and parameter estimation.

The choice of an appropriate distribution of probability to model data plays an important role in SAR image segmentation [3]. Our study adopts G_I^0 and G_A^0 distributions [3] to model SAR data in intensity and amplitude, respectively. The great advantage of using these distributions is that they can accurately model homogeneous, heterogeneous, and extremely heterogeneous regions of a SAR image [3]. In addition, other distributions such as K and Weibull do not present this feature.

Recent studies have shown that roughness information (i.e., texture) is an important and powerful attribute for edge detection [4] and segmentation [5] of SAR images. Here, we employ the roughness parameter maps estimated from data modeled by G_I^0 and G_A^0 distributions as inputs to achieve SAR image segmentation by using thresholding-based and level-set-based algorithms. For parameter estimation, we solve a nonlinear system of log cumulants of orders 1 and 2, for both aforementioned distributions. Inspired by [6], we use the idea introduced by Mejail *et al.* that the parameter estimation for each pixel may lead to estimated parameter maps that, in turn, can be used as inputs for classification methods, among other applications.

The structure of this letter is organized as follows. Section II briefly reviews SAR data modeling, and Section III presents the log-cumulants method (MoLC) for parameter estimation. In Section IV, we introduce the proposed methodology which provides the estimated roughness parameters of SAR data modeled by G_I^0 and G_A^0 distributions as inputs to segmentation algorithms. Section V presents the experimental results, and Section VI summarizes our findings and conclusions.

II. Statistical Models for SAR Data

Here, we investigate the class of G^0 distributions which consists of general models for SAR intensity (G_I^0) and amplitude (G_A^0) return data (Z). The probability density functions of G_I^0 and G_A^0 are defined as follows:

- G_I^0 distribution, i.e.,

$$f_{G_I^0}(z,\alpha,\gamma) = \frac{L^L\Gamma(L-\alpha)}{\gamma^\alpha\Gamma(-\alpha)\Gamma(L)} z^{L-1}(\gamma+Lz)^{\alpha-L} \quad (1)$$

Manuscript received May 25, 2015; revised September 29, 2015 and October 23, 2015; accepted October 24, 2015. Date of publication January 7, 2016; date of current version January 19, 2016.

The authors are with the Centro de Tecnologia, Universidade Federal do Ceará, 60455-760 Fortaleza-CE, Brazil, and also with Instituto Federal de Educação, Ciência e Tecnologia do Ceará, 60040-531 Fortaleza-CE, Brazil (e-mail: alixandreavila@yahoo.com.br; jeovafarias@gmail.com; regismarques@ifce.edu.br; fsombra@ufc.br; juvencio@ufc.br).

Digital Object Identifier 10.1109/LGRS.2015.2496340

where $\Gamma(L)$ refers to the Gamma function; $L \geq 1$ is the number of looks; $-\alpha, \gamma, z > 0$; and the rth-order moment is given by

$$E_{G_I^0}[Z^r] = \left(\frac{\gamma}{L}\right)^r \frac{\Gamma(-\alpha - r)\Gamma(L + r)}{\Gamma(-\alpha)\Gamma(L)}, \quad \alpha < -r \tag{2}$$

- G_A^0 distribution, i.e.,

$$f_{G_A^0}(z, \alpha, \gamma) = \frac{2L^L\Gamma(L - \alpha)}{\gamma^\alpha\Gamma(-\alpha)\Gamma(L)} z^{2L-1}(\gamma + Lz^2)^{\alpha - L} \tag{3}$$

where $-\alpha, \gamma, z > 0$; and the rth-order moment is given by

$$E_{G_A^0}[Z^r] = \left(\frac{\gamma}{L}\right)^{\frac{r}{2}} \frac{\Gamma\left(-\alpha - \frac{r}{2}\right)\Gamma\left(L + \frac{r}{2}\right)}{\Gamma(-\alpha)\Gamma(L)}, \quad \alpha < -\frac{r}{2}. \tag{4}$$

For both distributions, α and γ correspond to the roughness and scale parameters, respectively. The α parameter has immediate interpretation in terms of roughness, and therefore, it is regarded as a roughness or a texture measure [3], [6]. Here, the number of looks L is assumed to be known and constant for all pixels of the image.

III. Parameter Estimation

The parameter estimation for both G_I^0 and G_A^0 distributions is performed by MoLC, which is an alternative to the classical maximum-likelihood (ML) and method of moments (MoM) approaches [7]. Although the ML estimator has optimal properties (efficiency) under some regularity conditions, particularly in the exponential family, we did not use it due to certain limitations discussed in [8] and [9]. These limitations mainly involve complex analytic expressions for SAR data models, being necessary intensive numerical procedures to derive them. It is worth noting that MoM is very simple and fast to estimate; however, it has serious limitations [7], [10], [11].

On the other hand, MoLC generates strongly consistent estimators, including situations where MoM failed, and involves simpler algebraic operations than ML. Moreover, MoLC is computationally faster than ML, and it becomes particularly useful when the direct ML approach turns out to be unfeasible. Another important aspect for choosing MoLC is that the histogram of the estimated roughness parameters clearly indicates the number of regions present in the images, as depicted in Fig. 1. As a matter of fact, this histogram pattern is highly desirable to apply image segmentation methods based on thresholding.

MoLC is based on the Mellin transform of a probability density function, and it is defined by [8], [12]–[14]

$$\phi_z(s) = \mathcal{M}\left[p_z(u)\right] = \int_0^\infty u^{s-1} p_z(u) du \tag{5}$$

where s is a complex number with unity norm [8], and $p_z(u)$ is the probability density function of the random variable Z.

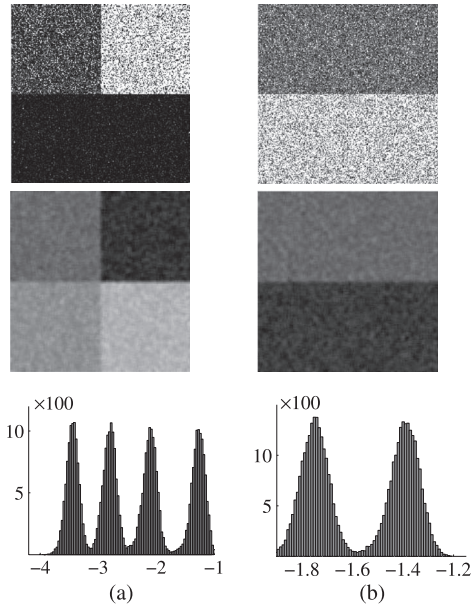

Fig. 1. (From top to bottom) Single-look synthetic SAR images, roughness maps estimated by MoLC, and roughness histograms. (a) Four-region intensity image simulated by using $\alpha \in \{-1.5, -3, -4.5, -6\}$ and (b) two-region amplitude image simulated by using $\alpha \in \{-1.5, -3\}$.

The Mellin transform of a function f only exists if f is defined over $\mathbb{R}^+$ [14], and the log cumulant of order v is defined as [8], [14]

$$\widetilde{k}_v = \left.\frac{d^v \psi_z(s)}{ds^v}\right|_{s=1}, \quad v \in \mathbb{N} \tag{6}$$

with $\psi_z(s) = \ln((\phi_z(s))$. Another important relation is that the log moment of order v can be obtained by

$$\widetilde{m}_v = \left.\frac{d^v \phi_z(s)}{ds^v}\right|_{s=1}, \quad v \in \mathbb{N}. \tag{7}$$

In this letter, we use the two log cumulants and log moments of orders 1 and 2, which are related by [8], [13]

$$\begin{cases} \widetilde{k}_1 = \widetilde{m}_1 \\ \widetilde{k}_2 = \widetilde{m}_2 - \widetilde{m}_1^2 \end{cases}. \tag{8}$$

The log cumulants of orders 1 and 2 for G_I^0 are given by [15]

$$\begin{cases} \widetilde{k}_1 = \log\left(\frac{\gamma}{L}\right) + \Psi^0(L) - \Psi^0(-\alpha) \\ \widetilde{k}_2 = \Psi^1(L) - \Psi^1(-\alpha) \end{cases} \tag{9}$$

and for G_A^0, the log cumulants of orders 1 and 2 are defined by [16]

$$\begin{cases} 2\widetilde{k}_1 = \log\left(\frac{\gamma}{L}\right) + \Psi^0(L) - \Psi^0(-\alpha) \\ 4\widetilde{k}_2 = \Psi^1(L) - \Psi^1(-\alpha) \end{cases} \tag{10}$$

where, in both distributions, $\Psi^0(\cdot)$ is the digamma function, and $\Psi^k(\cdot)$ is the digamma of kth order.

The strategy to estimate α and γ consists in solving the systems of nonlinear equations in (9) and (10), considering the

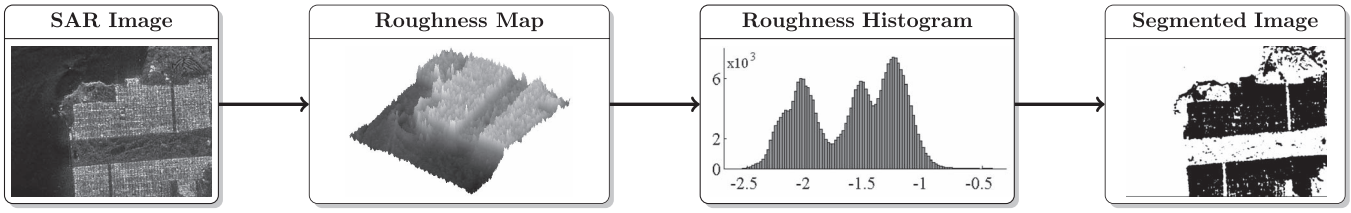

Fig. 2. Flowchart of the proposed methodology.

relations in (8) and replacing $\widetilde{m}_1$ and $\widetilde{m}_2$ by the corresponding sample log moments of orders 1 and 2, which are given by [8]

$$\widehat{\widetilde{m}}_v = \frac{1}{n}\sum_{i=1}^{n} \log z_i^v \tag{11}$$

with $z_i, i \in \{1, 2, \ldots, n\}$, being a sample of a random variable $Z \sim G_I^0$ or $Z \sim G_A^0$.

IV. Segmentation Methodology

The flowchart in Fig. 2 displays the methodology where the first step estimates roughness parameters by using MoLC. In the next step, the estimated parameters are inputs to segmentation algorithms, which can be also thresholding-based techniques. Our aim is to deliver a methodology for SAR segmentation that processes the roughness information or its histogram.

In order to investigate the technical feasibility of the proposed approach for SAR segmentation, we applied three algorithms introduced by Otsu [17], Huang *et al.* [18], and Marques *et al.* [19] directly to speckled images and to estimated roughness maps. The first method searches for a threshold value automatically, whereas the second one originally extracts a threshold value in a supervised manner, to guide the evolution of the level set front. The last one combines statistical properties of SAR data and level sets to derive a scheme that splits SAR images into different regions.

Here, we also proposed modified versions of the level-set-based algorithms. The method introduced in [18] relies on threshold values, which are manually defined, to guide the evolution of the level set front. In addition, this level set front evolves according to [18]

$$\begin{cases} F = I(x,y) - I_{\text{lower}}, & I(x,y) < I_{\text{average}} \\ I_{\text{high}} - I(x,y), & I(x,y) \geq I_{\text{average}} \end{cases} \tag{12}$$

where $I(x,y)$ denotes the pixel value at (x,y), I_{lower} and I_{high} are parameters which are set by the user, and I_{average} is the average of I_{lower} and I_{high}.

Then, we have replaced $I(x,y)$ by the roughness parameter map $M_\alpha(x,y)$ and adopted a single threshold T_α in (12) to avoid user intervention to set I_{lower} and I_{high} values. These modifications resulted in a modified version of the Huang *et al.* method, where F^* is a nonparametric version of F, and it is given by

$$F^* = \begin{cases} M_\alpha(x,y) - T_\alpha, & M_\alpha(x,y) < T_\alpha \\ T_\alpha - M_\alpha(x,y), & M_\alpha(x,y) \geq T_\alpha \end{cases} \tag{13}$$

where T_α is estimated by the Otsu method [17].

We applied the Otsu method directly to M_α, and furthermore, we used the Otsu's threshold of the roughness map as input to the Huang *et al.* method to guide the front evolution of this algorithm. Concerning the method introduced in [19], we replaced the original energy functional term by the roughness map. Then, the modified version of the propagation function in [19] is given by

$$F^* = -\frac{(M_\alpha - \mu_1)}{\mathcal{A}_1} + \frac{(M_\alpha - \mu_2)}{\mathcal{A}_2} \tag{14}$$

where the indexes 1 and 2 refer to background and foreground regions in the level set evolution. μ and $\mathcal{A}$ are the mean roughness and area of both regions, respectively.

Inspired by [20], we have adopted a 5×5 window size to estimate sample log moments. Frery *et al.* [20] have demonstrated that the larger the window size, the smoother the analysis, and thus concluded that most sites corresponded to heterogeneous or extremely heterogeneous spots. Moreover, when the window was small, more heterogeneous areas appeared.

A. Performance Evaluation of Segmentation

This letter applies the error of segmentation (EoS) measure to evaluate the proposed methodology on synthetic intensity and amplitude data segmentation. It is given by

$$\text{EoS} = \frac{\#(A)}{\#(\text{Image})} \tag{15}$$

where $\#(A)$ and $\#(\text{Image})$ stand for the number of mis-segmented pixels and the number of pixels of the whole image, respectively.

Two indexes quantify the segmentation accuracy and the difficulty of tests for experiments with real images. The first one is the cross-region fitting index, i.e., CRF [19]. It assesses segmentation results and takes values from the interval $[0, 1]$, where $\text{CRF} = 1$ indicates the best segmentation result. The second index concerns the difficulty of segmentation, i.e., DoS [19]. It quantifies the difficulty to segment SAR images based on the contrast between regions. As a matter of fact, both CRF and DoS indexes rely on a stochastic distance between two samples of regions which are modeled by G_I^0 or G_A^0 distributions [21].

V. Experimental Results

A. Synthetic Image Segmentation

The experiments were conducted on both synthetic intensity and amplitude SAR images which consist of two regions with

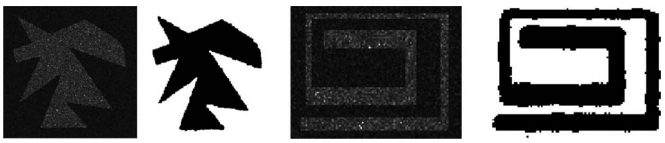

Fig. 3. Examples of the Monte Carlo experiment results.

TABLE I
EOS FOR THE OTSU METHOD

Roughness $(\alpha_b;\alpha_f)$	Otsu applied to	Intensity Image	Amplitude Image
$(-1.5;-4)$	M_α	0.0273 ± 0.0011	0.0296 ± 0.0105
	SAR data	0.7460 ± 0.0018	0.6909 ± 0.0019
$(-4;-8)$	M_α	0.0175 ± 0.0045	0.0520 ± 0.0089
	SAR data	0.7567 ± 0.0017	0.7225 ± 0.0021
$(-1.5;-8)$	M_α	0.0140 ± 0.0009	0.0146 ± 0.0026
	SAR data	0.2960 ± 0.0029	0.4734 ± 0.0035

different patterns, roughness parameters, and number of looks. We performed a Monte Carlo experiment with 10.000 intensity and amplitude images, respectively. To generate synthetic amplitude images, i.e., Z_A, we used the inverse transform method according to [19]. In addition, to generate intensity images, i.e., Z_I, we used the relation between amplitude and intensity data that states $Z_A^2 = Z_I$. Fig. 3 shows samples of synthetic speckled images.

Then, we investigated whether the methodology was suitable or not for SAR segmentation by applying threshold-based algorithms to synthetic images. Table I displays values for the mean EoS and standard deviation obtained with synthetic intensity and amplitude single-look SAR data and Otsu method. We performed the Monte Carlo experiments by using distinct roughness parameters for background (α_b) and foreground (α_f). With regard to the scale parameter, we adjusted it for background and foreground such that the first-order moment was equal to 1. Thus, we ensured segmentation of synthetic low-contrast images.

Table I displays highlighted values of EoS measure obtained by applying the Otsu method to roughness maps, whereas nonhighlighted values regard the results by applying the Otsu method directly to speckled images. These results confirmed that it is not feasible to apply threshold-based techniques directly to speckled images. However, when the input of the algorithm was the roughness map, it performed quite differently. We observed a similar performance with the Huang *et al.* method.

Fig. 4 shows the mean EoS values for synthetic SAR images with different roughness parameters and numbers of looks. Fig. 4(a) and (b) presents concisely the performance of the modified Otsu and Huang *et al.* methods, respectively.

These results demonstrated that the modified methods achieved minimum values of EoS for single-look images $(L = 1)$, which are markedly affected by the speckle. Furthermore, the performance of the proposed approach decreased substantially with the increase of the number of looks. The increment on the number of looks implies a reduction of both speckle variance and roughness information. Fig. 4(a) and (b) also illustrates how difficult it is to achieve segmentation in multilook synthetic SAR images by applying threshold-based algorithms to roughness information.

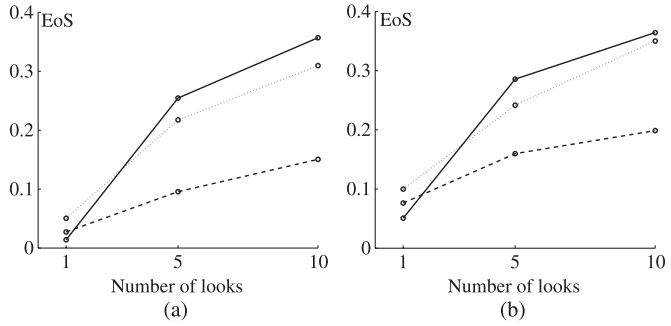

Fig. 4. Mean EoS for synthetic intensity SAR images with numbers of looks of 1, 5, and 10. (a) and (b) Results of the modified Otsu method and the modified Huang *et al.* method, respectively. Solid line refers to $(\alpha_b, \alpha_f) = (-1.5, -8)$, dash line to $(\alpha_b, \alpha_f) = (-1.5, -4)$, and dot line to $(\alpha_b, \alpha_f) = (-4, -8)$.

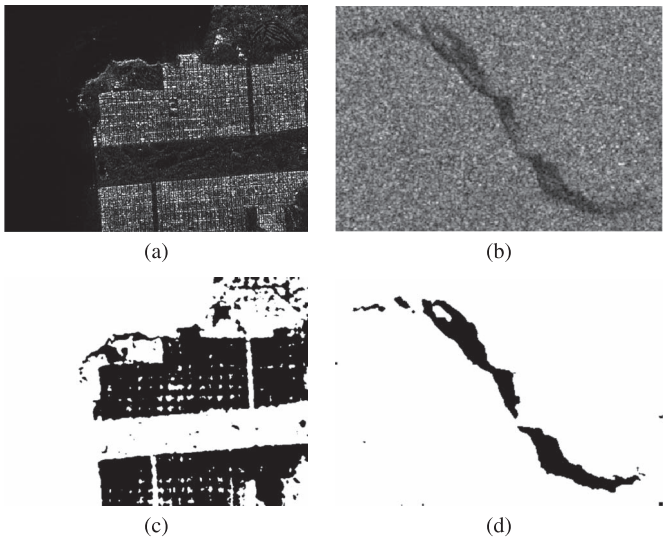

Fig. 5. Real SAR image segmentation. (a) Original image of San Francisco Bay. (b) Original image of oil slick and segmentation results by applying (c) modified Otsu [17] and (d) Marques *et al.* [19] methods.

B. Real SAR Image Segmentation

Tests with real SAR images included an intensity image with three looks and an amplitude image with four looks, both acquired at HH polarization. The intensity real SAR image in Fig. 5(a) was acquired by AIRSAR over San Francisco Bay. Fig. 5(b) shows a RADARSAT amplitude image of the Brazilian Northeast coast. This scene is over the Atlantic Ocean, and it consists of an oil slick.

Tables II and III present evaluation indexes values (CRF and DoS) for San Francisco and oil slick real images, respectively. The results demonstrated that the difficulty of segmentation of intensity real SAR images was greater than that of amplitude images. In fact, DoS measure is based on the contrast between regions, and intensity SAR images have lower contrast than amplitude images. With regard to CRF values, they were calculated from the results obtained with the methods introduced in [17]–[19] and their modified versions.

TABLE II
DoS AND CRF OF REAL IMAGE SEGMENTATION: SAN FRANCISCO

Image processed in	DoS	Segmentation approach	Methods		
			[17]	[18]	[19]
Intensity	2.9449	Original	0.2943	0.6058	0.6634
		Modified	0.6698	0.6431	0.6623
Amplitude	1.1714	Original	0.3670	0.6813	0.7452
		Modified	0.7515	0.7128	0.7407

TABLE III
DoS AND CRF OF REAL IMAGE SEGMENTATION: OIL SLICK

Image processed in	DoS	Segmentation approach	Methods		
			[17]	[18]	[19]
Intensity	2.4090	Original	0.2722	0.7472	0.8619
		Modified	0.8647	0.7702	0.8738
Amplitude	1.3911	Original	0.3503	0.7227	0.8914
		Modified	0.8638	0.7492	0.8813

From the CRF values, we concluded that our approach can be feasible for SAR image segmentation when applied to the roughness map estimated by MoLC. Furthermore, we observed that the processing results related to the method in [19] were quite similar regardless of using the original or its modified version.

With regard to the computational cost of the algorithms, we did not observe significant differences in processing a speckled image or its roughness map. Nevertheless, the roughness map estimation by MoLC was computationally expensive. In fact, the computational time to estimate M_α for the San Francisco and oil slick images was about 20 and 10 min, respectively. Comparing with MoM, the parameter estimation performed in [19] achieved 4.8 and 10.9 s, respectively. However, MoM failed in providing a roughness map without errors and thus required postprocessing. Although the roughness map estimation is computationally expensive, we emphasize the attractiveness and utility of M_α as input to challenging problems such as SAR segmentation, classification, and other applications.

VI. CONCLUSION

In this letter, we have introduced a methodology which used roughness information as input to segmentation algorithms instead of directly processing the speckled image. Our methodology relied on an appropriate statistical data modeling and parameter estimation to work reliably on SAR images. Thus, we adopted G_I^0 and G_A^0 distributions for data modeling and MoLC for parameter estimation. Our tests consist of segmentation algorithms based on thresholding and level set applied to synthetic and real SAR images. Although SAR image segmentation can be hard to achieve using thresholding-based techniques due to speckle, we showed that it can be suitable when applying these techniques to the estimated roughness parameters of G_I^0 and G_A^0. For single-look images, the results demonstrated that MoLC provided an estimated roughness map which clearly indicated the predominant regions present in the images. Hence, we concluded that our scheme can achieve promising segmentation results when applying thresholding-based and level-set-based techniques to the roughness parameter map. Another remarkable finding of this work is that it was indeed suitable for single-look image segmentation, i.e., the critical study case where the speckle and roughness information are stronger.

REFERENCES

[1] J. Kittler, J. Illingworth, and J. Föglein, "Threshold selection based on a simple image statistic," *Comput. Vis., Graph., Image Process.*, vol. 30, no. 2, pp. 125–147, May 1985.

[2] M. Sezgin and B. Sankur, "Survey over image thresholding techniques and quantitative performance evaluation," *J. Electron. Imag.*, vol. 13, no. 1, pp. 146–165, Jan. 2004.

[3] A. C. Frery, H.-J. Müller, C. C. Freitas, and S. J. S. Sant'Anna, "A model for extremely heterogeneous clutter," *IEEE Trans. Geosci. Remote Sens.*, vol. 35, no. 3, pp. 648–659, May 1997.

[4] L. Dias, F. C. Neto, and R. Ospina, "Interval edge estimation in SAR images," *IEEE Trans. Geosci. Remote Sens.*, vol. 53, no. 2, pp. 851–861, Feb. 2015.

[5] X. Tian, L. Jiao, L. Yi, K. Guo, and X. Zhang, "The image segmentation based on optimized spatial feature of superpixel," *J. Vis. Commun. Image Represent.*, vol. 26, pp. 146–160, Jan. 2015.

[6] M. E. Mejail, J. C. Jacobo-Berlles, and A. C. Frery, "Classification of SAR images using a general and tractable multiplicative model," *Int. J. Remote Sens.*, vol. 24, no. 18, pp. 3565–3582, 2003.

[7] V. Krylov, G. Moser, S. B. Serpico, and J. Zerubia, "On the method of logarithmic cumulants for parametric probability density function estimation," *IEEE Trans. Image Process.*, vol. 22, no. 10, pp. 3791–3806, Oct. 2013.

[8] J.-M. Nicolas, "Introduction aux statistiques de deuxième espèce: Application des logs-moments et des logs-cumulants à l'analyse des lois d'images radar," (in French), *Traitement du Signal*, vol. 19, no. 3, pp. 139–167, 2002.

[9] J. Feng and Z. Cao, "Multiphase SAR image segmentation with G^0 statistical-model-based active contours," *IEEE Trans. Geosci. Remote Sens.*, vol. 51, no. 7, pp. 4190–4199, Jul. 2013.

[10] E. L. Lehmann, *Elements of Large-Sample Theory*. New York, NY, USA: Springer-Verlag, 1999.

[11] P. K. Sen, J. M. Singer, and A. C. P. de Lima, *From Finite Sample to Asymptotic Methods in Statistics*. New York, NY, USA: Cambridge Univ. Press, 2010.

[12] G. Gao, X. Qin, and S. Zhou, "Modeling SAR images based on a generalized gamma distribution for texture component," *Progress Electromagn. Res.*, vol. 137, pp. 669–685, 2013.

[13] C. Tison, J. Marie, and F. Tupin, "A new statistical model for Markovian classification of urban areas in high-resolution SAR images," *IEEE Trans. Geosci. Remote Sens.*, vol. 42, no. 10, pp. 2046–2057, Oct. 2004.

[14] J. Cheng, G. Gao, W. Ding, X. Ku, and J. Sun, "An improved scheme for parameter estimation of G^0 distribution model in high-resolution SAR images," *Progress Eletromagn. Res.*, vol. 134, pp. 23–46, 2013.

[15] S. Cui and M. Datcu, "Coarse to fine patches-based multitemporal analysis of very high resolutions satellite images," in *Proc. 6th Int. Workshop Anal. Multi-Temporal Remote Sens. Images*, 2011, pp. 85–88.

[16] S. Cui, G. Schwarz, and M. Datcu, "A comparative study of statistical models for multilook SAR images," *IEEE Geosci. Remote Sens. Lett.*, vol. 11, no. 10, pp. 1752–1756, Oct. 2014.

[17] N. Otsu, "A threshold selection method from gray-level histograms," *IEEE Trans. Syst. Man Cybern.*, vol. 9, no. 1, pp. 62–66, Jan. 1979.

[18] B. Huang, H. Li, and X. Huang, "A level set method for oil slick segmentation in SAR images," *Int. J. Remote Sens.*, vol. 26, no. 6, pp. 1145–1156, Mar. 2005.

[19] R. C. P. Marques, F. N. Medeiros, and J. S. Nobre, "SAR image segmentation based on level set approach and G_A^0 model," *IEEE Trans. Pattern Anal. Mach. Intell.*, vol. 34, no. 10, pp. 2046–2057, Oct. 2012.

[20] A. C. Frery, F. C. Neto, and M. O. de Souza, "Analysis of minute features in speckled imagery with maximum likelihood estimation," *EURASIP J. Appl. Signal Process.*, vol. 2004, no. 1, pp. 2476–2491, Jan. 2004.

[21] A. D. C. Nascimento, R. J. Cintra, and A. C. Frery, "Hypothesis testing in speckle data with stochastic distances," *IEEE Trans. Geosci. Remote Sens.*, vol. 48, no. 1, pp. 373–385, Jan. 2010.